

**MICROSTRIP FILTER DESIGN  
USING DIRECT EM FIELD SIMULATION**

**J.W. Bandler, R.M. Biernacki, S.H. Chen,  
D.G. Swanson, Jr., and S. Ye**

**SOS-93-7-R**

**March 1993**

**(Revised July 1993)**

**© J.W. Bandler, R.M. Biernacki, S.H. Chen, D.G. Swanson, Jr., and S. Ye 1993**

**No part of this document may be copied, translated, transcribed or entered in any form into any machine without written permission. Address enquiries in this regard to Dr. J.W. Bandler. Excerpts may be quoted for scholarly purposes with full acknowledgement of source. This document may not be lent or circulated without this title page and its original cover.**



## **MICROSTRIP FILTER DESIGN USING DIRECT EM FIELD SIMULATION**

**John W. Bandler, Fellow, IEEE, Radoslaw M. Biernacki, Senior Member IEEE,  
Shao Hua Chen, Member, IEEE, Dan G. Swanson, Jr., Senior Member IEEE  
and Shen Ye, Member, IEEE**

### *Abstract*

For the first time we present minimax filter design with electromagnetic (EM) simulations driven directly by a gradient based optimizer. Challenges of efficiency, discretization of geometrical dimensions, and continuity of optimization variables are reconciled by a three stage attack: (1) efficient on-line response interpolation w.r.t. geometrical dimensions of microstrip structures simulated with fixed grid sizes, (2) smooth and exact gradient evaluation for use in conjunction with the proposed interpolation, and (3) storing the results of expensive EM simulations in a dynamically updated data base. Geometrical interpolation has been tested on a simple rectangular microstrip structure. Simulation of a low-pass microstrip filter illustrates the conventional use of EM simulation for design validation. Design optimization of a double folded stop-band filter and of a millimeter-wave 26-40 GHz interdigital capacitor band-pass microstrip filter illustrates the new technique.

---

J.W. Bandler, R.M. Biernacki and S.H. Chen are with Optimization Systems Associates Inc., P.O. Box 8083, Dundas, Ontario, Canada L9H 5E7, and with the Simulation Optimization Systems Research Laboratory, Department of Electrical and Computer Engineering, McMaster University, Hamilton, Canada L8S 4L7.

D.G. Swanson, Jr., is with Watkins-Johnson Company, Palo Alto, CA 94304-1204, USA.

S. Ye was with Optimization Systems Associates Inc., P.O. Box 8083, Dundas, Ontario, Canada L9H 5E7. He is now with Com Dev Ltd., Cambridge, Ontario, Canada N1R 7H6.

This work was supported in part by Optimization Systems Associates Inc. and in part by the Natural Sciences and Engineering Research Council of Canada under Grants OGP0007239, OGP0042444 and STR0117819 and through an Industrial Research Fellowship to S. Ye.

## I. INTRODUCTION

We present results of microwave filter design with accurate electromagnetic (EM) simulations driven by a minimax gradient based optimizer. We exploit recent advances [1-5] in EM simulation which give the designer the opportunity to accurately simulate passive circuit components, in particular microstrip structures [2]. However, we go far beyond the prevailing use of stand alone EM simulators, namely, validation of designs obtained through less accurate techniques.

EM simulators, though computationally intensive, are regarded as accurate at microwave frequencies, extending the validity of the models to higher frequencies, including millimeter-wave frequencies, and cover wider parameter ranges [2]. The EM simulators, whether stand-alone or incorporated into software frameworks, will not realize their full potential to the designer (whose task is to come up with the best parameter values satisfying design specifications) unless they are optimizer-driven to automatically adjust designable parameters.

Design optimization tools are widely available (e.g., [6]), typically in conjunction with analytical, heuristic models of microstrip structures developed in recent years. Consequently, designers, using such tools, try to generate designs in the form of either equivalent circuits, or physical parameters based on approximate models. Using an EM simulator, designers currently validate and improve their designs by manual adjustments. The need for direct design optimization with accurate field simulation is clear.

The feasibility of optimizing passive structures using EM simulation has already been shown by Jansen *et al.* [3,4]. Our paper addresses several challenges arising when EM simulations are to be put directly into the optimization loop. We consider the advantages of on-line EM simulations (performed on request) as opposed to up-front simulations, as in Jansen's look-up table approach. The requirement of circuit responses for continuously varying optimization variables must be reconciled with inherent discretization of geometrical parameters present in numerical EM simulations. Finally, the requirement of providing the optimizer with smooth and accurate gradient information must be given serious attention. We effectively deal with all these problems,

contributing a new dimension to this subject.

The concepts presented in this paper have been implemented in Empipe™ [7], an interface between OSA90/hope™ [8] and *em*™ [5]. On-line interpolation is applied to geometrical dimensions of microstrip structures to provide for continuity of optimization variables in the presence of fixed grid sizes in EM simulations. The results of EM simulations are stored in a data base and can be available if, during optimization, the same on-the-grid points need to be re-simulated.

The proposed geometrical interpolation has been tested on a simple rectangular microstrip structure. The conventional use of EM simulation for design validation is presented by comparing the results of *em* [5] simulation and the corresponding measurements of a low-pass microstrip filter. Design optimization of a double folded filter for stop-band applications and of a millimeter-wave 26-40 GHz interdigital capacitor microstrip band-pass filter illustrates the new technique.

Minimax design optimization is briefly reviewed in Section II. Section III includes our theory of geometrical interpolation and Section IV contains a derivation of gradient expressions for use in conjunction with geometrical interpolation. Storing the results of expensive EM simulations in a data base and issues of updating the data base are discussed in Section V. Finally, Sections VI to IX describe our experiments.

## II. MINIMAX DESIGN OPTIMIZATION

Frequency domain design of microwave filters involves design specifications imposed on the responses ( $S$  parameters, return loss, insertion loss, etc.). In order to formulate an objective function for design optimization the filter is simulated at a given point (vector) of designable (optimization) variables  $\phi$  and at the same frequency points at which the upper ( $S_{uj}$ ) and/or lower ( $S_{lj}$ ) specifications are selected. The corresponding responses, denoted by  $R_j(\phi)$ , determine the error vector  $e(\phi)$  as

$$e(\phi) = [e_1(\phi) \ e_2(\phi) \ \dots \ e_M(\phi)]^T \quad (1)$$

where the individual errors  $e_j(\phi)$  are of the form

$$e_j(\phi) = R_j(\phi) - S_{uj} \quad (2)$$

or

$$e_j(\phi) = S_{lj} - R_j(\phi) \quad (3)$$

and  $M$  is the total number of errors. A negative error value indicates that the corresponding specification is satisfied. For positive error values the corresponding specifications are violated. All the errors  $e_j(\phi)$  are combined into a single objective function to be minimized. Minimax design optimization is defined as

$$\underset{\phi}{\text{minimize}} \left( \max_j (e_j(\phi)) \right) \quad (4)$$

Effective minimax optimization requires a dedicated optimizer, such as [9], and accurate gradients of individual errors w.r.t. the optimization variables  $\phi$ .

### III. GEOMETRICAL INTERPOLATION

The vector  $\psi$  of all geometrical parameters (structure lengths, widths, spacings, etc.) of a planar microstrip structure can be written as

$$\psi = [\psi_{opt}^T(\phi) \quad \psi_{fix}^T]^T \quad (5)$$

where the vector  $\psi_{opt}(\phi)$  contains designable geometrical parameters which are either directly the optimization variables or are functions of the optimization variables  $\phi$ , and the vector  $\psi_{fix}$  contains fixed geometrical parameters. It is important to realize that each component of  $\psi$  belongs to one of the three physical orientations ( $x$ ,  $y$ , or  $z$ ) and, therefore, the vector  $\psi$  can be rearranged as

$$\psi = [\psi^{xT} \quad \psi^{yT} \quad \psi^{zT}]^T \quad (6)$$

Numerical EM simulation is performed for discretized values of geometrical parameters  $\psi$ . Let the discretization matrix  $\delta$  be defined by the grid sizes  $\Delta x_i$ ,  $\Delta y_i$  and  $\Delta z_i$  as

$$\delta = \text{diag}\{\delta_i\} = \text{diag}\{\Delta x_1, \Delta x_2, \dots, \Delta y_1, \Delta y_2, \dots, \Delta z_1, \Delta z_2, \dots\} \quad (7)$$

A specific EM simulator may allow only one grid size for each orientation while others may provide the flexibility of independent  $\Delta x_i$ ,  $\Delta y_i$  and  $\Delta z_i$  for different parameters of the same  $x$ ,  $y$ , or  $z$  orientation. For uniform discretization in each direction  $\Delta x_i = \Delta x$ ,  $\Delta y_i = \Delta y$  and  $\Delta z_i = \Delta z$ .

Before invoking EM simulation for a given  $\psi$  it is necessary to find "the nearest" point (vector) on the grid, denoted by  $\psi^c$ , which we call the *center base point*. We define it by the

equation

$$\boldsymbol{\psi} = \boldsymbol{\psi}^c + \boldsymbol{\delta} \boldsymbol{\theta} \quad (8)$$

subject to suitable conditions imposed on  $\boldsymbol{\theta}$  to precisely define the term "the nearest". For example, the conditions on  $\boldsymbol{\theta}$  can be chosen as

$$-0.5 \leq \theta_i < 0.5, \quad i = 1, 2, \dots, n \quad (9)$$

or as

$$0 \leq \theta_i < 1, \quad i = 1, 2, \dots, n \quad (10)$$

where  $n$  is the total number of geometrical parameters and  $\boldsymbol{\theta}$  is the relative deviation of  $\boldsymbol{\psi}$  from the center base point.  $\boldsymbol{\psi}^c$  and  $\boldsymbol{\theta}$  can be easily determined using the "floor" function as

$$\psi_i^c = \lfloor [\psi_i / \delta_i + 0.5] \rfloor \delta_i \quad \text{or} \quad \psi_i^c = \lfloor \psi_i / \delta_i \rfloor \delta_i \quad (11)$$

for (9) or (10), respectively, and

$$\theta_i = (\psi_i - \psi_i^c) / \delta_i \quad (12)$$

If  $\boldsymbol{\theta} \neq \mathbf{0}$  the point is off-the-grid and we use interpolation to determine each response  $R(\boldsymbol{\psi})$ . We drop the subscript  $j$  and take (5) into account in expressing  $R_j(\boldsymbol{\phi})$ . We consider the class of interpolation problems where the interpolating function can be expressed as a linear combination of some *fundamental interpolating functions* in terms of deviations w.r.t. the center base point. Let  $f(\boldsymbol{\delta\theta})$  be the vector of fundamental interpolating functions

$$f(\boldsymbol{\delta\theta}) = [f_1(\boldsymbol{\delta\theta}) \quad f_2(\boldsymbol{\delta\theta}) \quad \dots \quad f_K(\boldsymbol{\delta\theta})]^T \quad (13)$$

We want to find a vector

$$\mathbf{a} = [a_1 \quad a_2 \quad \dots \quad a_K]^T \quad (14)$$

such that

$$R(\boldsymbol{\psi}) - R(\boldsymbol{\psi}^c) = f^T(\boldsymbol{\delta\theta}) \mathbf{a} \quad (15)$$

holds exactly at  $K$  selected *base points*. Once  $\mathbf{a}$  is determined, (15) will be used to interpolate the response elsewhere in a suitably defined *interpolation region* around the center base point  $\boldsymbol{\psi}^c$ . The *interpolation base*  $B$  in the space of geometrical parameters is a set of grid points defined as

$$B = \{\boldsymbol{\psi}^c\} \cup \{\boldsymbol{\psi} \mid \boldsymbol{\psi} = \boldsymbol{\psi}^c + \mathbf{S} \boldsymbol{\delta} \boldsymbol{\eta}, \quad \boldsymbol{\eta} \in B^n\} \quad (16)$$

where

$$B^\eta = \{\eta^j \mid \eta^j \in I^n, \eta^j \neq \mathbf{0}, \eta^i \neq \eta^j, i, j = 1, 2, \dots, K\} \quad (17)$$

is a set of predefined integer vectors called *relative interpolation base*, and

$$\mathbf{S} = \text{diag}\{s_i\}, \quad \text{where} \quad s_i = \begin{cases} 1 & \text{if } \psi_i \text{ is a nonsymmetric parameter} \\ 2 & \text{if } \psi_i \text{ is a symmetric parameter} \end{cases} \quad (18)$$

The symmetry matrix  $\mathbf{S}$  accounts for double grid size increments for parameters whose dimensions are modified by extending or contracting both ends simultaneously.

The interpolation base  $B$  is used as the set of base points  $\psi^c$  and  $\psi^{bj}$ ,  $j = 1, 2, \dots, K$ , at which EM simulation is invoked to evaluate the corresponding set of responses  $R_{EM}(\psi^c)$ ,  $R_{EM}(\psi^{b1})$ , ...,  $R_{EM}(\psi^{bK})$ . From (15) we formulate a set of  $K$  linear equations

$$[\Delta R_{EM}(\psi^{b1}) \quad \Delta R_{EM}(\psi^{b2}) \quad \dots \quad \Delta R_{EM}(\psi^{bK})]^T = [f(\mathbf{S}\delta\eta^1) \quad f(\mathbf{S}\delta\eta^2) \quad \dots \quad f(\mathbf{S}\delta\eta^K)]^T \mathbf{a} \quad (19)$$

where  $\Delta R_{EM}(\psi^{bj}) = R_{EM}(\psi^{bj}) - R_{EM}(\psi^c)$ . More concisely

$$\Delta R_{EM}(B) = F(\mathbf{S}\delta, B^\eta) \mathbf{a} \quad (20)$$

By solving (20) we determine the vector  $\mathbf{a}$  of interpolation coefficients as

$$\mathbf{a} = F^{-1}(\mathbf{S}\delta, B^\eta) \Delta R_{EM}(B) \quad (21)$$

which, after substituting into (15), gives

$$R(\psi) = R_{EM}(\psi^c) + f^T(\delta\theta) F^{-1}(\mathbf{S}\delta, B^\eta) \Delta R_{EM}(B) \quad (22)$$

(22) provides the response values for the off-the-grid points. Note that the matrix  $F(\mathbf{S}\delta, B^\eta)$  in (20) must be invertible. This, however, depends only on the selection of the fundamental interpolating functions and the relative interpolation base  $B^\eta$  and can be determined prior to all calculations. It is also independent of the center base point, so the same formulas are involved as the variables move during optimization.

#### IV. GRADIENT ESTIMATION

To facilitate the use of an efficient and robust dedicated gradient minimax optimizer we need to provide the gradients of the errors (2) and (3), or the gradients of  $R_j(\phi)$ . From (5) we can determine

$$\nabla_\phi R_j(\phi) = \nabla_\phi \psi^T(\phi) \nabla_\psi R(\psi) \quad (23)$$

The first factor on the right hand side of (23) is readily available since the mapping (5), as an integral part of the problem formulation, is known. The second factor on the right hand side of (23) must be determined using EM simulations.

During optimization it is very likely that the gradient will be requested at off-the-grid points. As discussed in the preceding section the responses at off-the-grid points are determined by interpolation. It is, therefore, most appropriate from the optimizer's point of view to provide the gradient of the interpolating function, i.e., the function that is actually returned to the optimizer. This is fortunate since that gradient can be analytically derived from the fundamental interpolating functions. From (22) we get

$$\nabla_{\psi} R(\psi) = \nabla_{\delta\theta} f^T(\delta\theta) F^{-1}(\mathcal{S}\delta, B^{\eta}) \Delta R_{EM}(B) \quad (24)$$

Equation (24) gives accurate gradient information for the optimizer in a simple, straightforward and efficient manner. Note that  $F^{-1}(\mathcal{S}\delta, B^{\eta})$  and  $\Delta R(B)$  are already available from response interpolation.

Some optimizers may request perturbed simulation in the vicinity of the nominal point  $\phi^0$ , say at  $\phi^{pert}$ , in order to estimate the gradient by perturbation, instead of using the gradient at  $\phi^0$  directly. In such cases, using (22) at  $\phi^{pert}$  may provide a different result from (24) unless the fundamental interpolating functions are linear. As the exact gradient (24) is available, a modified response at  $\phi^{pert}$  can be easily evaluated from the linearized interpolating function at  $\phi^0$  as

$$R(\psi^{pert}) = R_{EM}(\psi^c) + [f^T(\delta\theta^0) + (\psi^{pert} - \psi^0)^T \nabla_{\delta\theta} f^T(\delta\theta^0)] F^{-1}(\mathcal{S}\delta, B^{\eta}) \Delta R_{EM}(B) \quad (25)$$

where  $\psi^0$ ,  $\theta^0$  and  $\psi^{pert}$  are determined from  $\phi^0$  and  $\phi^{pert}$ , respectively. This formula, when used in gradient estimation by perturbation, will produce the same result as (24).

## V. UPDATING THE DATA BASE OF SIMULATED RESULTS

In order to efficiently utilize the results of EM simulations and to reduce their number we have considered two levels of control. First, interpolation is invoked only when necessary, i.e., if a specific  $\theta_i$  is zero we exclude the corresponding base point from the interpolation base. To be able to implement such a scheme the fundamental interpolating functions must be appropriately

devised. Secondly, a data base  $D$  of base points and the corresponding responses obtained from exact EM simulations is stored and accessed when necessary (see Fig. 1). Each time EM simulation is requested the corresponding interpolation base  $B$  is generated and checked against the existing data base. Actual EM simulation is invoked only for the base points not present in the data base ( $B - D$ ). Results for the base points already present in the data base ( $B \cap D$ ) are simply retrieved from  $D$  and used for interpolation.

Updating the data base  $D$  is a separate issue. Between the two extremes: (1) all simulated results are saved, and (2) only results for the latest interpolation base are saved, many schemes can be adopted depending on such factors as required memory, access time, repeated simulations, etc. In any case, however, it is worthwhile to remember the current (active) interpolation base. This is particularly useful in (25), even if the perturbed point falls outside the interpolation region.

## VI. SIMULATION OF A SIMPLE MICROSTRIP STRUCTURE

The proposed geometrical interpolation has been implemented in Empipe [7] interfacing our general purpose CAD system OSA90/hope [8] with *em* [5]. On-line interpolation is performed on the structure responses w.r.t. geometrical dimensions which in *em* are discretized, that is snapped to the grid.

A simple microstrip rectangular structure shown in Fig. 2 (D'Inzeo, *et al.* [10]) was simulated to verify the geometrical interpolation technique and its software implementation. Simulation was carried out from 2 GHz to 18 GHz with a 0.1 GHz step on a Sun SPARCstation 1. Fig. 3 shows the simulated  $|S_{21}|$  in dB vs. frequency. These results are very close to the measurement data [10]. It should also be noted that agreement as good as this could not be achieved with traditional empirical microstrip equivalent circuit models.

## VII. EXPERIMENTAL VALIDATION OF A MICROSTRIP FILTER DESIGN

A conventional, and until now state-of-the-art, use of EM simulation to validate designs obtained by means other than direct optimization is illustrated by measurements and EM simulation of the low-pass microstrip filter shown in Fig. 4. The filter was designed by first synthesizing an LC prototype, and secondly by designing the corresponding microstrip components to match those of the prototype.

The filter was then built on a 25 mil thick alumina substrate with a relative dielectric constant of 9.8. The rectangular inductors utilized air bridges with vias, were made of 2 mil wide lines with 1 mil gaps and occupied a total area of 19 mils  $\times$  16 mils. The center capacitor had dimensions of 50  $\times$  115 mils and the end capacitors 35  $\times$  74 mils (the value of 75 mils was used for simulation). The measurements on the filter were taken at frequencies from 0.2 GHz to 11.8 GHz with a step of 0.2 GHz. The measured  $|S_{11}|$  and  $|S_{21}|$  vs. frequency are shown in Fig. 5 together with the corresponding plots obtained by electromagnetic simulation using *em* [5].

Using a Sun SPARCstation 2, simulation was carried out for the same frequency range from 0.2 GHz to 11.8 GHz with a step of 0.2 GHz. For simulation, the whole structure was partitioned into individual components: capacitors and inductors, the latter including the connecting transmission lines. Because of symmetry only one inductor and one end capacitor were simulated. Additional pieces of transmission lines were added for each component and de-embedded for better accuracy and to account for discontinuities at both sides of each capacitor.

The simulation times were approximately 100 seconds for the inductor, 10 seconds for the center capacitor and 8 seconds for the end capacitor, all per one frequency point. The resulting *S* parameters of the individual components were then combined to determine the *S* parameters of the overall filter. The results, though not as good as desirable at very low frequencies (below 300 MHz) give a very good approximation of filter behaviour in all critical areas, in particular around the cut-off frequency. The discrepancies between measured and simulated  $|S_{11}|$  at very low frequencies may be due to numerical problems in EM simulation that becomes apparent when vias are electrically very short.

## VIII. DESIGN OF DOUBLE FOLDED MICROSTRIP STRUCTURE

A double folded stub microstrip structure for band-stop filter applications, shown in Fig. 6, may substantially reduce the filter area while achieving the same goal as the conventional double stub structure shown in Fig. 7 [11]. The symmetrical double folded stub can be described by 4 parameters: width, spacing and two lengths  $W$ ,  $S$ ,  $L_1$  and  $L_2$ , as marked in Fig. 6.

We used minimax optimization, with  $W$  fixed at 4.8 mils and  $L_1$ ,  $L_2$  and  $S$  as variables, to move the center frequency of the stop band from 15 GHz to 13 GHz starting from the values given by [11]. Design specifications were taken as

$$|S_{21}| > -3 \text{ dB} \quad \text{for } f < 9.5 \text{ GHz and } f > 16.5 \text{ GHz}$$

$$|S_{21}| < -30 \text{ dB} \quad \text{for } 12 \text{ GHz} < f < 14 \text{ GHz}$$

The substrate thickness and the relative dielectric constant were 5 mils and 9.9, respectively.

Using OSA90/hope [8] and *em* [5] interfaced through Empipe [7], optimization was carried out in two steps. First, we applied identical  $\Delta x = \Delta y = 2.4$  mils grid size in both  $x$  and  $y$  directions. Then the grid size was reduced to  $\Delta x = \Delta y = 1.6$  mils for fine resolution. The values of the optimization variables before and after optimization are reported in Table I. Figs. 8(a) and 8(b) show  $|S_{21}|$  in dB vs. frequency before and after optimization, respectively.

## IX. DESIGN OF AN INTERDIGITAL MICROSTRIP FILTER

A 26-40 GHz millimeter-wave bandpass filter [12] was built on a 10 mils thick substrate with relative dielectric constant of 2.25. The filter, shown in Fig. 9, utilized thin microstrip lines and interdigital capacitors to realize inductances and capacitances of a synthesized lumped ladder circuit. The filter was designed to satisfy the specifications

$$|S_{11}| < -20 \text{ dB}$$

$$|S_{21}| > -0.04 \text{ dB}$$

for  $26 \text{ GHz} < f < 40 \text{ GHz}$ . The original microstrip design was determined by matching the lumped prototype at the center frequency using *em* [5]. However, when the filter was simulated by *em* in the whole frequency range the results exhibited significant discrepancies w.r.t. the prototype. It

necessitated manual adjustment and made a satisfactory design very difficult to achieve. The filter was then built and measured [12].

As for the double folded microstrip structure, design of the interdigital filter was carried out using *em* [5] driven by the minimax gradient optimizer of OSA90/hope [8] through Empipe [7]. There was a total of 13 designable parameters including the distance between the patches  $L_1$ , the finger length  $L_2$  and two patch widths  $W_1$  and  $W_2$  for each of the three interdigital capacitors, and the length  $L$  of the end capacitor, as shown in Fig. 9. The transmission lines between the capacitors were fixed at the originally designed values. The second half of the circuit, to the right of the plane of symmetry, is assumed identical to the first half, so it contains no additional variables.

A typical minimax equal-ripple response of the filter was achieved after a series of consecutive optimizations with different subsets of optimization variables and frequency points [13]. The filter was then built with the resulting geometrical dimensions rounded to 0.1 mil resolution. Fig. 10 shows the corresponding simulated and measured filter responses: magnitudes of  $S_{11}$  and  $S_{21}$ . Recent improvements in the field solver analysis of interdigital capacitors will improve the accuracy of the bandwidth prediction of Fig. 11(a). Also, the insertion loss flatness (Fig. 11(b)) will clearly improve after return loss has been tuned.

## X. CONCLUSIONS

For the first time we have presented a comprehensive approach to microwave filter design which exploits accurate field simulations driven directly by a powerful gradient based minimax optimizer. The benefits of electromagnetic simulations are thus significantly extended. Our approach, illustrated by simulation of two microstrip structures and the minimax design of two filters, paves the way for direct use of field theory based simulation in practical optimization-driven microwave circuit design.

## ACKNOWLEDGEMENT

The authors thank Dr. J.C. Rautio of Sonnet Software, Inc., Liverpool, NY. His initiatives, encouragement and help substantially facilitated this timely and important work.

## REFERENCES

- [1] J.C. Rautio and R.F. Harrington, "An electromagnetic time-harmonic analysis of arbitrary microstrip circuits," *IEEE Trans. Microwave Theory Tech.*, vol. 35, 1987, pp. 726-730.
- [2] T. Itoh, Ed., *Numerical Techniques for Microwave and Millimeter-Wave Passive Structures*. New York: Wiley, 1989.
- [3] R.H. Jansen and P. Pogatzki, "A hierarchically structured, comprehensive CAD system for field theory-based linear and nonlinear MIC/MMIC design," *1992 2nd Int. Workshop of the German IEEE MTT/AP Joint Chapter on Integrated Nonlinear Microwave and Millimeterwave Circuits Dig.* (Duisburg, Germany), 1992, pp. 333-341.
- [4] *LINMIC+/N Version 3.0*, Jansen Microwave, Bürohaus am See, Am Brüll 17, W-4030 Ratingen 1, Germany, 1992.
- [5] *Em User's Manual*, Sonnet Software, Inc., Suite 203, 135 Old Cove Road, Liverpool, NY 13090-3774, May 1992.
- [6] J.W. Bandler and S.H. Chen, "Circuit optimization: the state of the art," *IEEE Trans. Microwave Theory Tech.*, vol. 36, 1988, pp. 424-443.
- [7] *Empipe™ Version 1.0 Technical Brief*, Optimization Systems Associates Inc., P.O. Box 8083, Dundas, Ontario, Canada L9H 5E7, 1992.
- [8] *OSA90/hope™ Version 2.0 User's Manual*, Optimization Systems Associates Inc., P.O. Box 8083, Dundas, Ontario, Canada L9H 5E7, 1992.
- [9] J.W. Bandler, W. Kellermann and K. Madsen, "A superlinearly convergent minimax algorithm for microwave circuit design," *IEEE Trans. Microwave Theory Tech.*, vol. MTT-33, 1985, pp. 1519-1530.
- [10] G. D'Inzeo, F. Giannini, C.M. Sodi and R. Sorrentino, "Method of analysis and filtering properties of microwave planar networks," *IEEE Trans. Microwave Theory Tech.*, vol. MTT-26, 1978, pp. 462-471.
- [11] J.C. Rautio, Sonnet Software, Inc., 135 Old Cove Road, Suite 203, Liverpool, NY 13090-3774, Private communication, 1992.
- [12] D.G. Swanson, Jr., Watkins-Johnson Company, 3333 Hillview Avenue, Stanford Research Park, Palo Alto, CA 94304-1204, Private communication, 1992.
- [13] J.W. Bandler, S.Ye, R.M. Biernacki, S.H. Chen and D.G Swanson, Jr., "Minimax microstrip filter design using direct EM field simulation," *IEEE MTT-S Int. Microwave Symp. Dig.* (Atlanta, GA), 1993, pp. 889-892.

**TABLE I**  
**PARAMETER VALUES FOR THE DOUBLE FOLDED STUB**  
**BEFORE AND AFTER OPTIMIZATION**

---

| Parameter | Before optimization<br>(mil) | After optimization<br>(mil) |
|-----------|------------------------------|-----------------------------|
| $L_1$     | 74.0                         | 91.82                       |
| $L_2$     | 62.0                         | 84.71                       |
| $S$       | 13.0                         | 4.80                        |

---

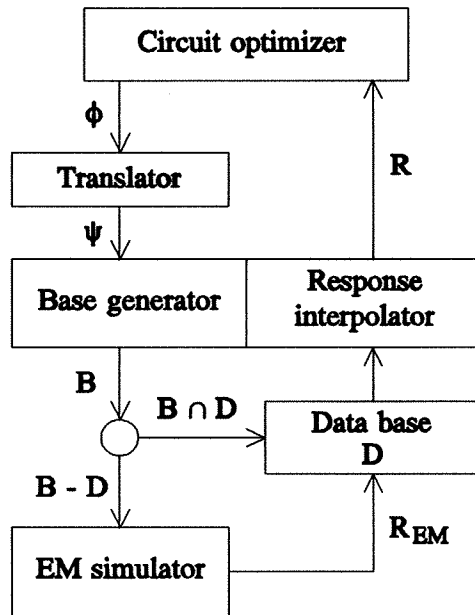


Fig. 1. Flow diagram illustrating the interconnection between a circuit optimizer and a numerical EM simulator.

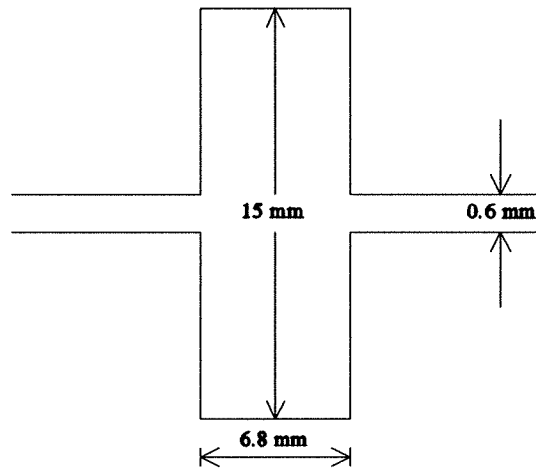


Fig. 2. A microstrip rectangular structure [9]. The thickness and dielectric constant of the substrate are 0.635 mm and 10.0, respectively.

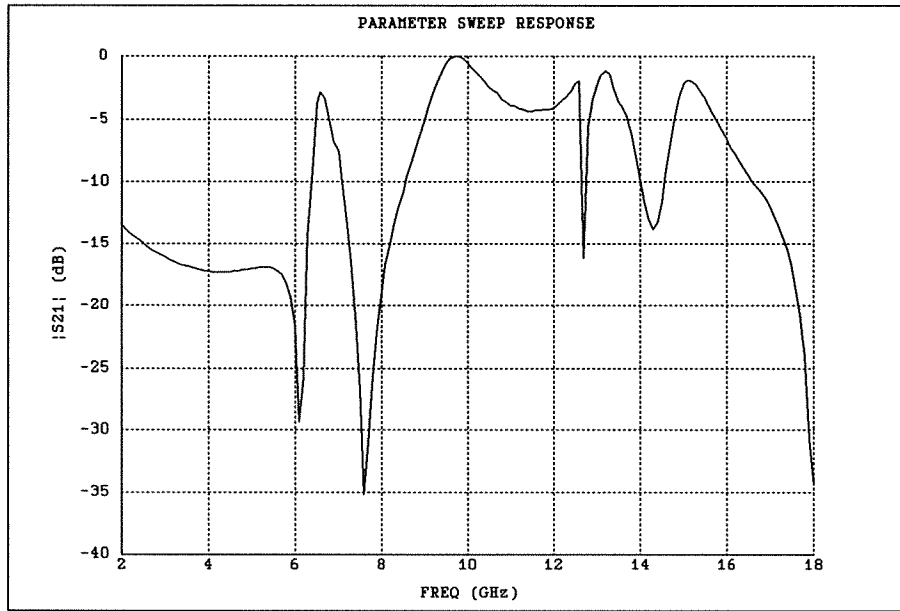


Fig. 3.  $|S_{21}|$  in dB vs. frequency for the rectangular structure.

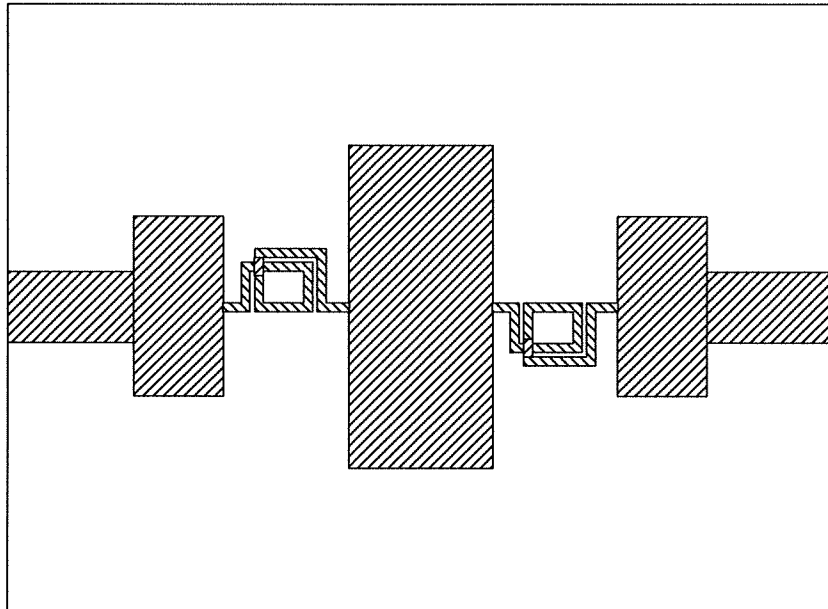


Fig. 4. Low-pass microstrip filter. The thickness and dielectric constant of the substrate are 25 mils and 9.8, respectively.

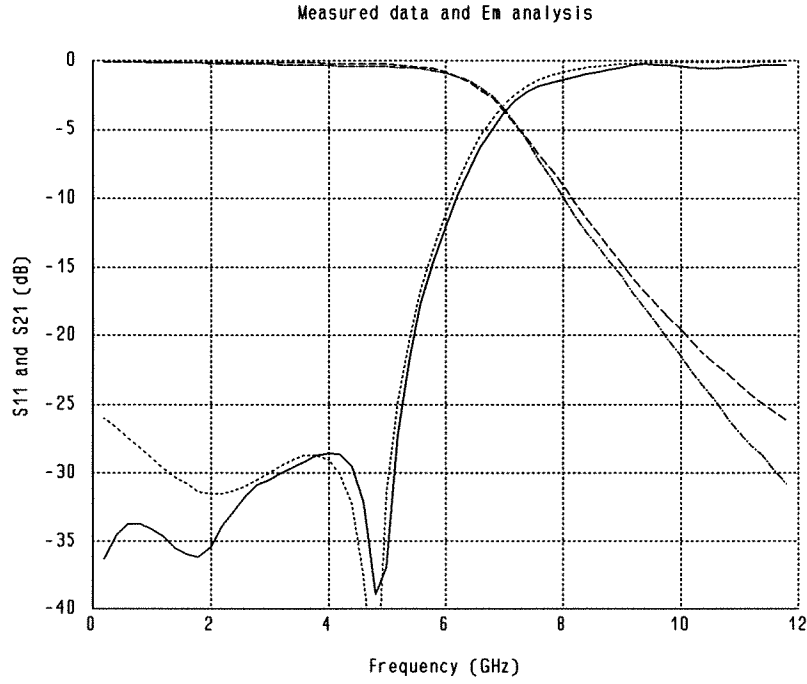


Fig. 5. EM simulation and measurements of the low-pass filter: (---) simulated  $|S_{11}|$ , (-·-·-) measured  $|S_{11}|$ , (.....) simulated  $|S_{21}|$ , and (—) measured  $|S_{21}|$ .

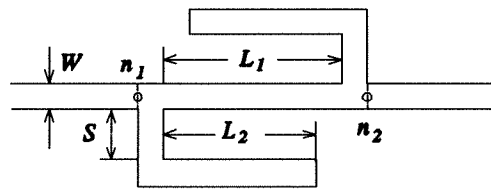


Fig. 6. Double folded stub microstrip structure for band-stop filter applications.

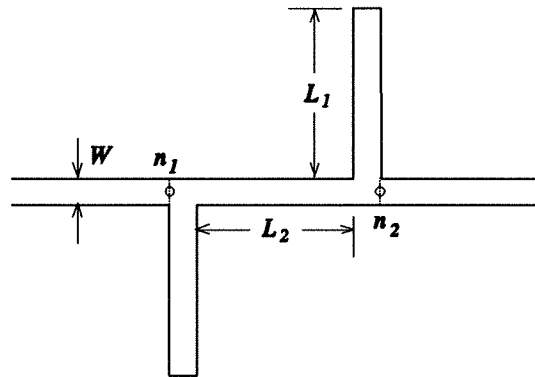
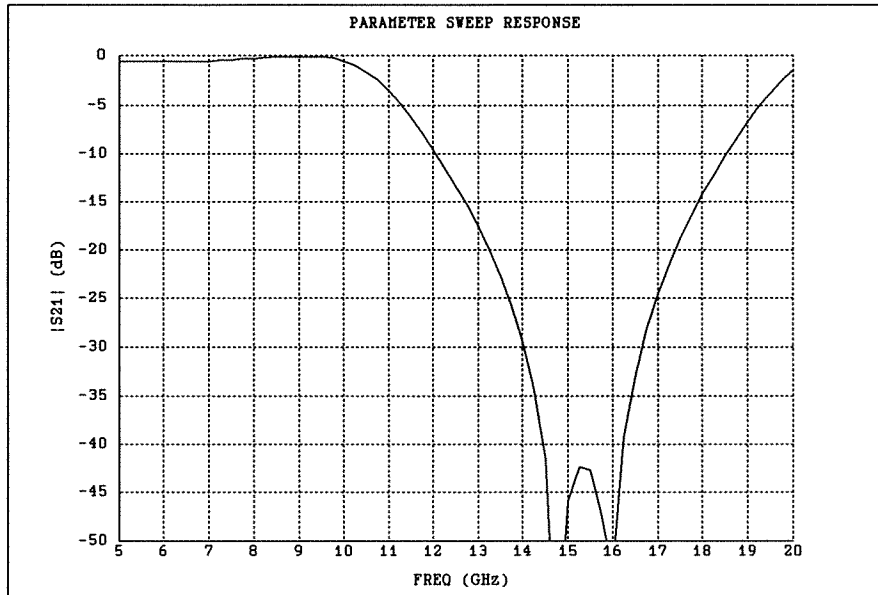
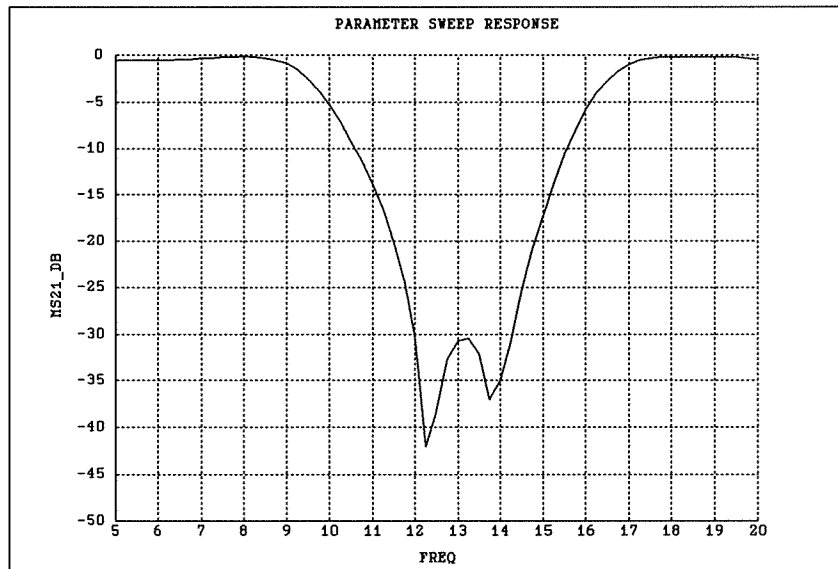


Fig. 7. Double stub microstrip structure.



(a)



(b)

Fig. 8. Double folded stub band-stop filter structure simulation, (a) before optimization, and (b) after optimization.

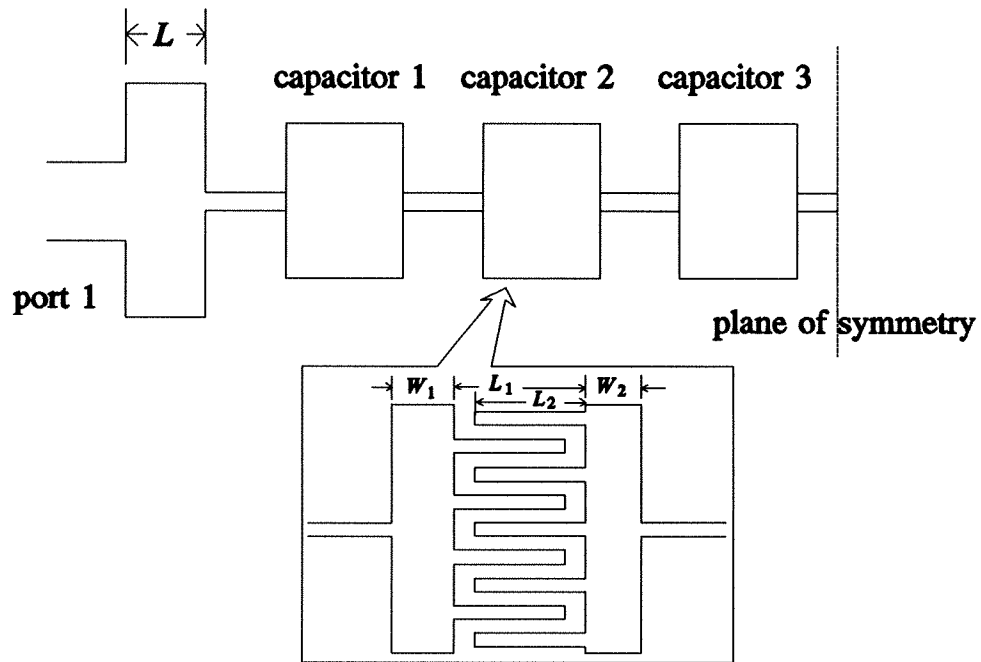
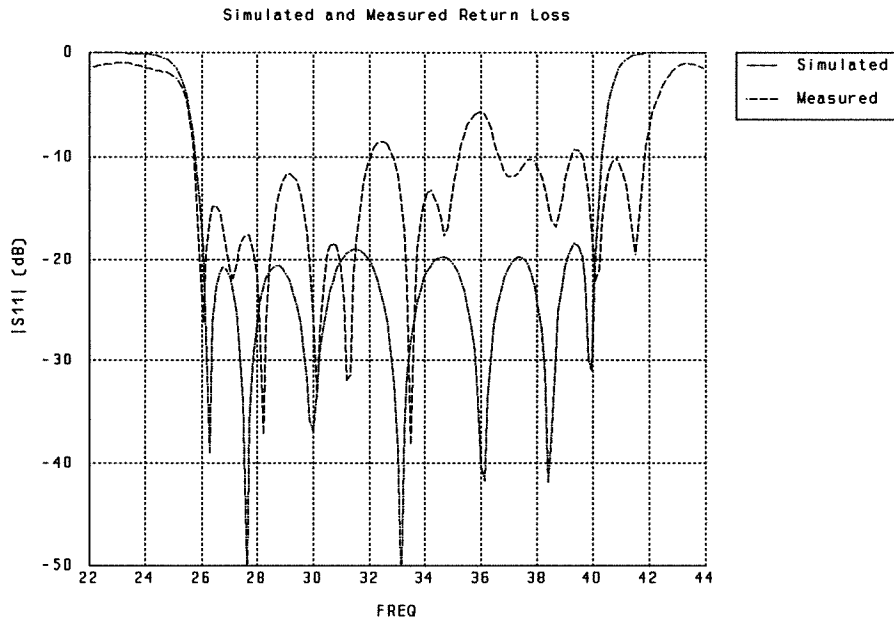
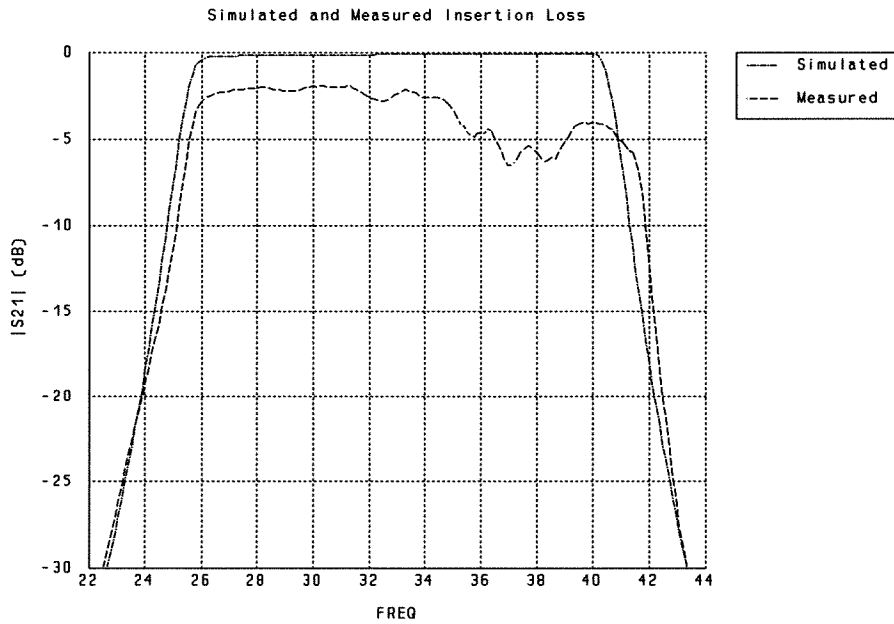


Fig. 9. The 26-40 GHz interdigital capacitor filter. The dielectric constant is 2.25. Substrate thickness and shielding height are 10 and 120 mils, respectively. The optimization variables include  $L$ , and  $L_1$ ,  $L_2$ ,  $W_1$ ,  $W_2$  for each capacitor, totalling 13.



(a)



(b)

Fig. 10. 26–40 GHz interdigital capacitor filter after minimax optimization and fabrication. All the optimization variables have been rounded to 0.1 mil resolution. Measured (---) and simulated (----): (a) magnitude of  $S_{11}$ , and (b) magnitude of  $S_{21}$ .